JACS
JOURNAL OF THE AMERICAN CHEMICAL SOCIETY
Communication
pubs.acs.org/JACS
Open Access on 08/15/2015

# The Cyanide Ligands of [FeFe] Hydrogenase: Pulse EPR Studies of $^{13}C$ and $^{15}N$-Labeled H-Cluster

William K. Myers,[†,§] Troy A. Stich,[†,§] Daniel L. M. Suess,[†] Jon M. Kuchenreuther,[†] James R. Swartz,[‡] and R. David Britt*[,†]

[†]Department of Chemistry, University of California, Davis, Davis, California 95616 United States

[‡]Department of Chemical Engineering and Department of Bioengineering, Stanford University, Stanford, California 94305 United States

Supporting Information

**ABSTRACT:** The two cyanide ligands in the assembled cluster of [FeFe] hydrogenase originate from exogenous L-tyrosine. Using selectively labeled tyrosine substrates, the cyanides were isotopically labeled via a recently developed *in vitro* maturation procedure allowing advanced electron paramagnetic resonance techniques to probe the electronic structure of the catalytic core of the enzyme. The ratio of the isotropic $^{13}C$ hyperfine interactions for the two $CN^-$ ligands—a reporter of spin density on their respective coordinating iron ions—collapses from ≈5.8 for the $H_{ox}$ form of hydrogenase to <2 for the CO-inhibited form. Additionally, when the maturation was carried out using [$^{15}N$]-tyrosine, no features previously ascribed to the nitrogen of the bridging dithiolate ligand were observed suggesting that this bridge is not sourced from tyrosine.

Hydrogenases catalyze the redox interconversion of protons and $H_2$ and thus have received much focus as key elements in biological solar fuel production.[1] The [FeFe] form of hydrogenase (HydA) is particularly active,[1] and its catalytic H-cluster consists of a [4Fe-4S] cluster ($[4Fe\text{-}4S]_H$) linked through a cysteine sulfur to a unique dinuclear iron cluster ($[FeFe]_H$, Scheme 1).[2] This subcluster possesses five inorganic ligands—two $CN^-$ and three CO—as well as a bridge recently assigned as dithiomethylamine (DTMA).[3,4]

Active HydA can be expressed in *Escherichia coli* only by also adding genes for three Fe-S containing maturase enzymes—HydE, HydF, and HydG—that are required for production of the $[FeFe]_H$ subcluster.[5] Alternatively, synthetic dinuclear Fe clusters can be transferred to HydA apoprotein (containing only the $[4Fe\text{-}4S]_H$ subcluster) to produce active enzyme.[4] We are utilizing a different technology: the HydE, HydF, and HydG maturases are added to a solution of apo-HydA for *in vitro* maturation and concurrent activation.[6] This cell-free biosynthetic method allows for facile and precise isotope incorporation into the $[FeFe]_H$ subcluster.[7]

The Fe-bound CO and $CN^-$ ligands of the $[FeFe]_H$ subcluster are sourced from L-tyrosine (Tyr) and produced by HydG.[8−10] In the present study, we use the cell-free biosynthetic method along with $\alpha$-$^{13}C$-Tyr ([2-$^{13}C$]-Tyr) and [$^{15}N$]-Tyr to specifically label the two $CN^-$ ligands with the magnetic nuclei $^{13}C$ and $^{15}N$ ($I$ = 1/2).[11,12] The hyperfine interaction (HFI) of these magnetic nuclei with the unpaired electrons distributed over the H-cluster serve as site-specific reporters of its electronic structure, important metrics for evaluating computational models of the H-cluster.

When poised in the active oxidation state known as $H_{ox}$, the $[4Fe\text{-}4S]_H$ subcluster is diamagnetic with a formal charge of 2+,[13] though the $[4Fe\text{-}4S]_H$ carries some unpaired density due to the exchange interaction with the $[FeFe]_H$ fragment. $[FeFe]_H$ itself is in a formally mixed-valence Fe(I,II) $S$ = 1/2 state that is characterized by a rhombic electron paramagnetic resonance (EPR) spectrum (Figure 1A, top). While the overall oxidation state of the $H_{ox}$ form of the H-cluster is widely accepted, the distribution of the valences about the cluster is still debated. One formulation based on results from electronic structure calculations assigns a 1+ oxidation state to the Fe that is distal to the $[4Fe\text{-}4S]_H$ subcluster ($Fe_d$), leaving the proximal Fe ion ($Fe_p$) in the ferrous oxidation state.[14] However, $^{57}Fe$ electron nuclear double resonance (ENDOR) spectroscopic studies of HydA from *Desulfovibrio desulfuricans* (*DdS*) found that the spin density was shared more-or-less equally over both iron ions of $[FeFe]_H$.[15] Many computational models of the H-cluster have been judged based on the quality of the predicted magnetic parameters. Initially, only the $^{57}Fe$ HFI were employed as a discriminating constraint.[14,16] More recently, however, ligand HFI, from either the nearby, naturally abundant $^{14}N$ nuclei or from $^{13}C$ nuclei introduced by treatment of HydA with isotopically labeled $^{13}CO$ gas, have been used to evaluate computer-generated structural models of the H-cluster.[3,16,17] Unfortunately, in the case of the $^{14}N$ hyperfine parameters, the assignment of the observed signals to

Scheme 1

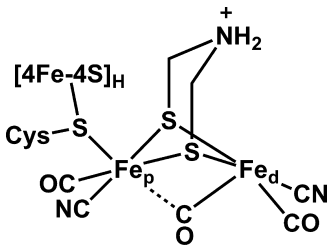


Received: July 11, 2014
Published: August 15, 2014


© 2014 American Chemical Society

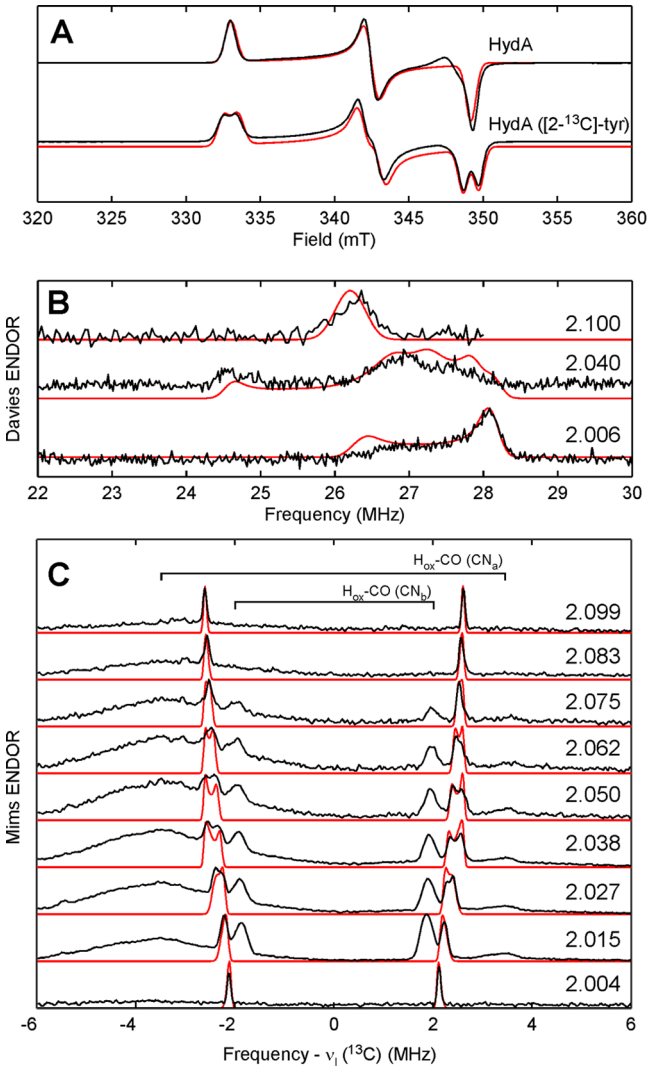


**Figure 1.** X-band (9.4 GHz) CW EPR spectra (A) of the $H_{ox}$ form of HydA matured using natural-abundance Tyr (top) or [2-$^{13}$C]-Tyr (bottom). Davies ENDOR spectra (B) of HydA ([2-$^{13}$C]-Tyr) collected at 1158, 1192, and 1212 mT (top to bottom). Corresponding *g*-values given in figure. Q-band (33.79 GHz) Mims ENDOR spectra (C) of HydA ([2-$^{13}$C]-Tyr) collected at 1150, 1157, 1164, 1171, 1178, 1184, 1191, 1198, and 1205 mT (top to bottom). Corresponding *g*-values given in figure. Traces of experimental data are shown in black; simulations for the $H_{ox}$ form are presented in red.

specific nitrogen atoms is ambiguous owing to the high natural-abundance of $^{14}$N; and the $^{13}$CO-treatment aids only in characterizing the $H_{ox}$-CO form. We therefore reasoned that studies of the electronic structure of $H_{ox}$ would be aided by selective incorporation of magnetic nuclei into the diatomic ligands of the $[FeFe]_H$ cluster.

The X-band continuous-wave (CW) EPR spectrum of *in vitro* matured HydA from *Clostridium pasteurianum* (CpI) poised in the $H_{ox}$ state is consistent with that published previously with *g* = 2.100, 2.040, 1.996 (Figure 1A). Using [2-$^{13}$C]-Tyr in the maturation of HydA leads to a splitting of ≈1 mT centered at each *g*-value of this $H_{ox}$ signal (cf. top and bottom traces in Figure 1A).[18] Q-band Davies ENDOR spectra acquired at field positions corresponding to each *g*-value (Figure 1B) confirm this strong $^{13}$C HFI by showing features at ≈27 MHz that have no counterpart in analogous spectra of HydA matured using natural-abundance tyrosine.[19] The variation in shape and breadth of these features as a function of resonant field position results from orientation selection, i.e., at certain field positions, a discrete subset of molecular orientations of HydA are probed. Proper simulation of this behavior allows for the orientation of the corresponding $^{13}$C hyperfine tensor to be determined relative to the molecular *g*-tensor. These parameters are summarized in Table 1. The degree of $^{13}$C HFI anisotropy is consistent with that of other Fe-bound cyanides (cf. Table 1).

Orientation-selected Mims ENDOR spectra (Figure 1C) reveal three distinct classes of more weakly coupled $^{13}$C nuclei ($A_{iso}$ = 3.80, 4.87, and ≈7.0 MHz). These features are centered about the $^{13}$C Larmor frequency and split by the magnitude of the HFI. Analogous data sets collected for CO-treated samples (Figures S3 and S4) possess similar features at ±1.8 and ±3.6 MHz, confirming that they arise from the two cyanide ligands in the $H_{ox}$-CO form of hydrogenase (labeled as $CN_a$ and $CN_b$ since we cannot distinguish between the $Fe_p$-bound and $Fe_d$-bound cyanides at this time). Note the absence of contributions from $H_{ox}$-CO to the ENDOR spectra acquired at the extreme field positions (*g* = 2.099 and 2.004) of $H_{ox}$ (Figure 1C). This results from the relative narrowness of the $H_{ox}$-CO signal. This narrowness is also why we see strong contributions from $H_{ox}$-CO even though the contamination is relatively small. The remaining features centered at ±2.2 MHz in Figure 1C are thus ascribed to the other $CN^-$ ligand in $H_{ox}$.

Based on the crystallographic results,[2] $Fe_d$ possesses a square pyramidal local geometry whose *z*-axis points along the bond between the $Fe_d$ ion and the bridging CO. For the six-coordinate $Fe_p$, the identity of the local *z*-axis is less obvious, but computational results suggest that it is aligned along the $Fe_p$-$CO_{bridge}$ bond.[14] As the two terminal $CN^-$ ligands appear to be bound in the same position relative to the local *z*-axis of their respective Fe ions, the ratio of the isotropic $^{13}$C HFI should serve as a reporter of the relative spin density on each iron. Again, based on earlier computational results, we assign the larger $^{13}$C HFI as arising from the distal Fe-bound cyanide of $H_{ox}$. For the proximal Fe-bound cyanide, we measure $A_{iso}$ = 4.87 MHz. This ratio of ≈5.8 correlates approximately with the $Fe_d$:$Fe_p$ ratio of computed Mulliken spin populations.[14,16] For $H_{ox}$–CO, the $A_{iso}(^{13}CN_a)$:$A_{iso}(^{13}CN_b)$ ratio drops to <2 (see magnetic parameters listed in Table 1) indicating a much more even distribution of spin density over the two Fe ions than what was observed for $H_{ox}$ that is again consistent with computational results.[14,16] Interestingly, the $^{13}$C HFI tensors for the two $CN^-$ ligands in the $H_{ox}$–CO form lack significant anisotropy compared to other Fe-bound cyanides (cf. Table 1)

X- and Q-band HYSCORE spectra for natural-abundance $H_{ox}$ (Figure 2, top) are essentially identical to those obtained earlier by Silakov et al.[3] When the *in vitro* maturation of HydA is performed with $^{15}$N-labeled tyrosine ([$^{15}$N]-Tyr), the nitrogens of the cyanide ligands become selectively isotopically labeled.[9] The corresponding HYSCORE data are strikingly different from those of natural-abundance $H_{ox}$ (cf. top and bottom plots in Figure 2) signaling that the majority of features arise from tyrosine-derived nitrogens. The correlation ridges in the Q-band spectrum of $H_{ox}$ ([$^{15}$N]-Tyr) are well-simulated with the hyperfine parameters $A(^{15}N)$ = [0.8, 6.3, −1.2] MHz (Figure S5). Given the rather large magnitude of $A_{iso}(^{15}N)$, this nitrogen is likely that in the $Fe_d$-bound cyanide. We observe no $^{15}$N-derived features that we could assign to cyanides in the $H_{ox}$–CO form.


dx.doi.org/10.1021/ja507046w | J. Am. Chem. Soc. 2014, 136, 12237−12240

**Table 1. $^{13}$C HFI and $^{15}$N HFI for CO and CN Bound to Fe-Centers**

| species | $A^{13}$C (MHz) | [$\alpha$, $\beta$, $\gamma$] (deg)[a] | assignment | reference |
|---|---|---|---|---|
| CpI $H_{ox}$ ([2-$^{13}$C]-Tyr) | [30.9, 23.3, 30.2] | [60, 120, 170] | $CN_d$ | this work |
| | [5.22, 5.24, 4.16] | [30, 90, 0] | $CN_p$ | this work |
| CpI $H_{ox}$-CO ([2-$^{13}$C]-Tyr) | [7.0, 7.0, 7.2] | [0, 0, 0] | $CN_a$ | this work |
| | [3.75, 3.75, 3.90] | [0, 0, 0] | $CN_b$ | this work |
| *DdS* $H_{ox}$-$^{13}$CO | [15.6, 16.6, 19.2] | | $CO_{ext}$ | 17 |
| | [8.5, 9.8, 3.9] | | $CO_{bridge}$ | 17 |
| | [3.2, 3.7, 4.4] | | $CO_d$ | 17 |
| Mb-$^{13}$CN | [−23.0, −27.6, −28.7] | | Fe(III)-CN | 21 |
| *Pf* Fd-$^{13}$CN | [−4.5, −4.5, +0.1] | | [4Fe-4S]$^+$-CN | 22 |
| species | $A^{15}$N (MHz) | [$\alpha$, $\beta$, $\gamma$] (deg) | assignment | reference |
| CpI $H_{ox}$ ([$^{15}$N]-Tyr) | [0.8, 6.3, −1.2] | [45, −20, 0] | $CN_d$ | this work |
| *DdS* $H_{ox}$ | [2.1, 5.3, −0.6][b] | [41, 24, 0] | $CN_d$ | 3 |
| | [1.4, 2.7, 2.0][b] | [40, 25, 0] | DTMA | 3 |
| | [−3.4, 2.0, −1.0][b] | [0, 4, 20] | Lys | 3 |
| *DdS* $H_{ox}$-CO | [0.56, −0.28, 0.79][b] | [0, −10, 0] | | 17 |
| Mb-C$^{15}$N | [n.d., n.d., 5.25] | | Fe(III)-CN | 23 |
| *Pf* Fd-C$^{15}$N | [+1.8, +1.0, −2.4] | | [4Fe-4S]$^+$-CN | 22 |

[a]Euler angles are relative to *g*-frame defined by $g1 < g2 < g3$. For $H_{ox}$, this corresponds to $g_z < g_y < g_x$ as we assign the local *z*-axis of $Fe_d$ to the Fe-$CO_{bridge}$ bonding vector. [b]Determined by scaling the experimentally determined $^{14}$N HFI by the ratio of the $^{15}$N/$^{14}$N Larmor frequencies (1.4028). [c]Abbreviations: Mb = myoglobin; *Pf* Fd = [4Fe-4S] ferredoxin from *Pyrococcus furiosus*; n.d. = not determined.

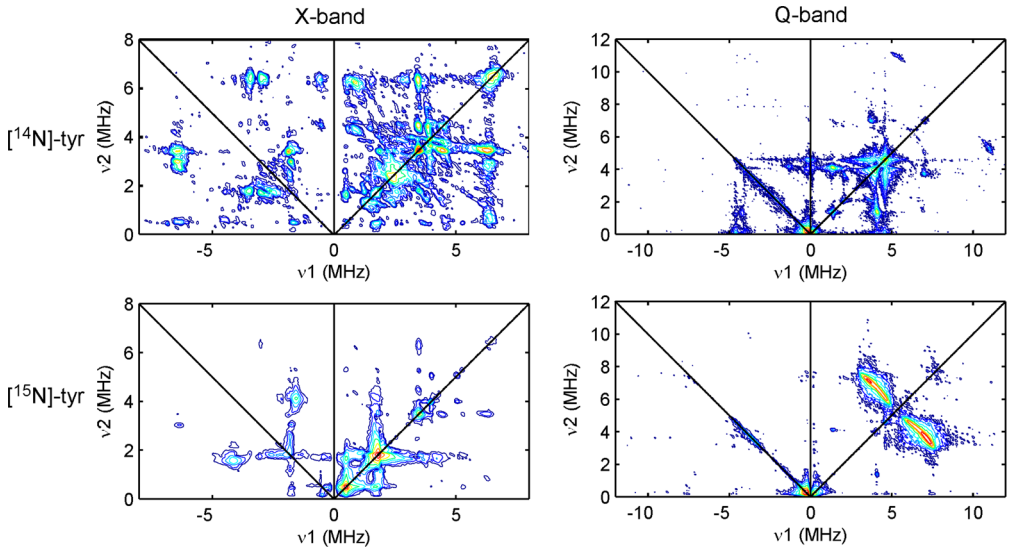


**Figure 2.** X-band (left) and Q-band (right) HYSCORE spectra of the $H_{ox}$ form of HydA matured using natural-abundance ([$^{14}$N]-Tyr, top) or with [$^{15}$N]-Tyr (bottom).

The biosynthetic origin of the putative DTMA bridge is presently unknown. One proposal suggests that HydG can assemble this bridging ligand from two molecules of tyrosine.[20] Analysis of $^{14}$N HYSCORE spectra of *DdS* HydA poised in the $H_{ox}$ state led to the assignment of a set of correlation ridges to the DTMA amino nitrogen ($A(^{14}N)$ = [1.0, 1.9, 1.4] MHz).[3] By scaling this reported $^{14}$N HFI by the ratio of the $^{15}$N/$^{14}$N Larmor frequencies, we can simulate the X-band HYSCORE spectrum as if the DTMA had been $^{15}$N-labeled (see Figures S6 and S7). The predicted correlation ridges corresponding to the $^{15}$N-DTMA nitrogen are not found in the experimental HYSCORE spectrum of $H_{ox}$ ([$^{15}$N]-Tyr) suggesting either that tyrosine is not the source of the DTMA nitrogen or that the previously reported $^{14}$N HFI parameters for *DdS* HydA are not appropriate for CpI $H_{ox}$.

Using isotopically labeled tyrosine substrates in conjunction with the *in vitro* biosynthetic route to generate the H-cluster gives us the flexibility to site-specifically label the cyanide ligands with $^{13}$C and $^{15}$N. The signals we observe from $^{15}$N are unambiguously attributed to the nitrogen of an Fe-bound cyanide. Further, comparison of the two cyanide $^{13}$C couplings is consistent with just one of the Fe ions ($Fe_d$) of $[FeFe]_H$ carrying the majority of unpaired electron spin in the $H_{ox}$ state. As such, the relatively large rhombicity of the $H_{ox}$ EPR signal can be understood as arising from the asymmetry in the equatorial ligand set for the low-spin $3d^7$ $Fe_d$ spin center. Thus, the difference in *g*-shifts for $g_y$ and $g_x$ (0.0367 vs 0.0947) is attributed to the difference in the energies of the $Fe_d$-$3d_{xz}$ → $Fe_d$-$3d_{z^2}$ and the $Fe_d$-$3d_{yz}$ → $Fe_d$-$3d_{z^2}$ transitions, respectively.[24] If we orient the *g*-tensor for $H_{ox}$ as follows: $g_z$ is oriented along of *z*-axis of $Fe_d$, and $g_x$ and $g_y$ are made to bisect the $Fe_d$-S and $Fe_d$-S bonding vectors and the $Fe_d$-$CO_d$ and $Fe_d$-$CN_d$ bonding vectors, respectively; then the unique axis of the $^{13}$C hyperfine tensor for $CN_d$ is found to point approximately along the $Fe_d$-


dx.doi.org/10.1021/ja507046w | J. Am. Chem. Soc. 2014, 136, 12237−12240

$CN_d$ bond, as expected (Figure S8).[25] This finding supports our electronic structure description of $H_{ox}$; namely, that the unpaired electron largely resides in a molecular orbital of $3d_{z^2}$ character centered on the $Fe_d$ ion.

Based on the similar magnitudes of the $^{13}CN$ HFI, the electron spin becomes distributed more evenly over both iron ions after inhibition with free CO. This more delocalized spin topology leads to a collapse of the *g*-matrix rhombicity. Analogously, the rather narrow EPR signal for the formally mixed-valence Cu(I,II) $Cu_A$ cluster in nitrous oxide reductase is understood as a weighted sum of the hypothetical mononuclear *g*-matrices of each Cu site.[26] In the case of $H_{ox}$-CO, we do not know the values for the intrinsic *g*-matrix for the two Fe ions. However, we can use the $H_{ox}$ *g*-values as a first estimate. Upon forming $H_{ox}$-CO, delocalization of the unpaired electron spin cancels out some of the anisotropy from each site-specific *g*-matrix, leading to the axial ($g$ = 2.072, 2.006, 2.006), molecular *g*-matrix. The nearly isotropic HFI tensors for the two $CN^-$ ligands in $H_{ox}$-CO result from this same mechanism of anisotropy cancellation. These findings are in agreement with earlier computational models[14,16] that indicate a dramatic delocalization of unpaired spin density in going from the $H_{ox}$ form to $H_{ox}$-CO

## ■ ASSOCIATED CONTENT

### Supporting Information

Details of experimental procedures and data analysis methods. Supplemental EPR spectra and corresponding simulations. This material is available free of charge via the Internet at http://pubs.acs.org.

## ■ AUTHOR INFORMATION


### Corresponding Author

rdbritt@ucdavis.edu

### Author Contributions

[§]These authors contributed equally.


### Notes

The authors declare no competing financial interest.

## ■ ACKNOWLEDGMENTS

This work was funded by National Institutes of Health (GM104543 to R.D.B.) and the Division of Material Sciences and Engineering (J.R.S. award no. DE-FG02-09ER46632) of the Office of Basic Energy Sciences of the U.S. Department of Energy. D.L.M.S. acknowledges support from the National Institutes of Health (F32GM111025 from the NIGMS).

## ■ REFERENCES


(1) Vincent, K. A.; Parkin, A.; Armstrong, F. A. *Chem. Rev.* **2007**, *107*, 4366.

(2) Peters, J. W.; Lanzilotta, W. N.; Lemon, B. J.; Seefeldt, L. C. *Science* **1998**, *282*, 1853.

(3) Silakov, A.; Wenk, B.; Reijerse, E.; Lubitz, W. *Phys. Chem. Chem. Phys.* **2009**, *11*, 6592.

(4) Berggren, G.; Adamska, A.; Lambertz, C.; Simmons, T. R.; Esselborn, J.; Atta, M.; Gambarelli, S.; Mouesca, J. M.; Reijerse, E.; Lubitz, W.; Happe, T.; Artero, V.; Fontecave, M. *Nature* **2013**, *499*, 66.

(5) Shepard, E. M.; Mus, F.; Betz, J. N.; Byer, A. S.; Duffus, B. R.; Peters, J. W.; Broderick, J. B. *Biochemistry* **2014**, *53*, 4090.

(6) Kuchenreuther, J. M.; Shiigi, S. A.; Swartz, J. R. *Methods Mol. Biol. (N. Y., NY, U. S.)* **2014**, *1122*, 49.

(7) Kuchenreuther, J. M.; Myers, W. K.; Suess, D. L. M.; Stich, T. A.; Pelmenschikov, V.; Shiigi, S. A.; Cramer, S. P.; Swartz, J. R.; Britt, R. D.; George, S. J. *Science* **2014**, *343*, 424.

(8) Swanson, K. D.; Duffus, B. R.; Beard, T. E.; Peters, J. W.; Broderick, J. B. *Eur. J. Inorg. Chem.* **2011**, 935.

(9) Kuchenreuther, J. M.; George, S. J.; Grady-Smith, C. S.; Cramer, S. P.; Swartz, J. R. *PLoS One* **2011**, *6*, e20346.

(10) Kuchenreuther, J. M.; Myers, W. K.; Stich, T. A.; George, S. J.; NejatyJahromy, Y.; Swartz, J. R.; Britt, R. D. *Science* **2013**, *342*, 472.

(11) Driesener, R. C.; Challand, M. R.; McGlynn, S. E.; Shepard, E. M.; Boyd, E. S.; Broderick, J. B.; Peters, J. W.; Roach, P. L. *Angew. Chem.* **2010**, *49*, 1687.

(12) Shepard, E. M.; Duffus, B. R.; George, S. J.; McGlynn, S. E.; Challand, M. R.; Swanson, K. D.; Roach, P. L.; Cramer, S. P.; Peters, J. W.; Broderick, J. B. *J. Am. Chem. Soc.* **2010**, *132*, 9247.

(13) Popescu, C. V.; Munck, E. *J. Am. Chem. Soc.* **1999**, *121*, 7877.

(14) Fiedler, A. T.; Brunold, T. C. *Inorg. Chem.* **2005**, *44*, 9322.

(15) Silakov, A.; Reijerse, E. J.; Albracht, S. P. J.; Hatchikian, E. C.; Lubitz, W. *J. Am. Chem. Soc.* **2007**, *129*, 11447.

(16) Greco, C.; Silakov, A.; Bruschi, M.; Ryde, U.; De Gioia, L.; Lubitz, W. *Eur. J. Inorg. Chem.* **2011**, 1043.

(17) Silakov, A.; Wenk, B.; Reijerse, E.; Albracht, S. P. J.; Lubitz, W. *J. Biol. Inorg. Chem.* **2009**, *14*, 301.

(18) A modest (20% of overall spectral intensity) of the axial signal ($g$ = 2.072, 2.006, 2.006) arising from $H_{ox}$-CO was removed by subtraction. $H_{ox}$-CO contamination is common and can be seen by other methods such as infrared absorption spectroscopy.[9]

(19) This ENDOR transition at 27 MHz is approximately equal to twice the $^{13}C$ Larmor frequency at this field; therefore the ENDOR transtion in other spin manifold is expected at <1 MHz though it is not evident in our ENDOR data. However, both $^{13}C$ spin-flip transitions are observed in the Q-band HYSCORE spectrum (Figure S2).

(20) Pilet, E.; Nicolet, Y.; Mathevon, C.; Douki, T.; Fontecilla-Camps, J. C.; Fontecave, M. *FEBS Lett.* **2009**, *583*, 506.

(21) Van Doorslaer, S.; Trandafir, F.; Harmer, J. R.; Moens, L.; Dewilde, S. *Biophys. Chem.* **2014**, *190*−*191*, 8.

(22) Telser, J.; Smith, E. T.; Adams, M. W. W.; Conover, R. C.; Johnson, M. K.; Hoffman, B. M. *J. Am. Chem. Soc.* **1995**, *117*, 5133.

(23) Mulks, C. F.; Scholes, C. P.; Dickinson, L. C.; Lapidot, A. *J. Am. Chem. Soc.* **1979**, *101*, 1645.

(24) Weil, J. A.; Bolton, J. R. *Electron paramagnetic resonance: elementary theory and practical applications*; John Wiley & Sons: Hoboken, NJ, 2007.

(25) Telser, J.; Smith, E. T.; Adams, M. W. W.; Conover, R. C.; Johnson, M. K.; Hoffman, B. M. *J. Am. Chem. Soc.* **1995**, *117*, 5133.

(26) Neese, F.; Zumft, W. G.; Antholine, W. E.; Kroneck, P. M. H. *J. Am. Chem. Soc.* **1996**, *118*, 8692.